PCCP

PAPER

View Article Online
View Journal | View Issue

Published on 17 April 2019. Downloaded by CONSIGLIO NAZIONALE DELLE on 3/14/2022 6:54:14 PM.

Check for updates

Cite this: *Phys. Chem. Chem. Phys.*, 2019, **21**, 9987

Ultrafast photodissociation dynamics of pyrazole, imidazole and their deuterated derivatives using *ab initio* multiple cloning†

Christopher C. Symonds, *[ab] Dmitry V. Makhov,[ac] Neil C. Cole-Filipiak, ‡[d] James A. Green, §[a] Vasilios G. Stavros[d] and Dmitrii V. Shalashilin*[a]

Received 3rd January 2019,
Accepted 17th April 2019

DOI: 10.1039/c9cp00039a

rsc.li/pccp

We present results obtained using the *ab initio* multiple cloning (AIMC) method to simulate fully quantum dynamics for imidazole and its structural isomer pyrazole along with their selectively deuterated species. We simulate the ultrafast dissociation of the N–H/D bond for these molecules along the repulsive $^1\pi\sigma^*$ state which agrees well with previous experimental results. Our results give evidence for a two-stage dissociation of the N–H/D bond on the sub-50 fs regime for imidazole, pyrazole and their selectively deuterated species, and give evidence for the importance of the repulsive $^1\pi\sigma^*$ state along the N–H/D bond coordinate for the relaxation of both imidazole and pyrazole. The ability of these calculations to reproduce experimental results lends confidence that larger complex systems could be explored with predictive capabilities with the AIMC method. These results also confirm the ability of the AIMC method to add detailed insights into which experiments are blind.

1 Introduction

Nitrogen containing aromatic heterocycles are found throughout nature in various biologically significant molecules and compounds. The imidazole molecule for example is prevalent as a subunit in important biological compounds including fluorescent proteins, purines such as the DNA bases adenine and guanine, and amino acids such as histidine. Due to this prevalence of imidazole, in recent years there has been significant interest in investigating its ultrafast excited state dynamics following photo-absorption both experimentally[1–10] and theoretically.[8,11–14] Pyrazole, a structural isomer of imidazole rarely found in biomolecules, has been less widely studied both experimentally[3,15,16] and theoretically[17] and thus is, along with imidazole, the subject of a comparative experimental and nonadiabatic quantum dynamics study in the present work. The effect of selective deuteration at the N–H bond has also been studied experimentally,[3,15] but not theoretically, so we also model this for both molecules.

Initially, it is worthwhile to briefly summarise the current understanding of the ultrafast excited state dynamics of both molecules. Imidazole is an aromatic heterocycle containing two non-adjacent nitrogen atoms at the 1 and 3 positions of the aromatic ring. The seminal work by Sobolewski *et al.*[18] identified the importance of low lying $\pi\sigma^*$ states in aromatic heterocycles, showing them to be dissociative along the N–H stretch coordinate and providing an ultrafast radiationless transfer route through a conical intersection with the ground state, deactivating on an ultrafast time scale and providing a key clue to photoprotection in nature. Numerous studies have indicated that this non-radiative relaxation can play a part in photoprotection processes within biological systems.[2,4,10] As with other aromatic heterocycles, the lowest energy $\pi\sigma^*$ state ($1^1A''$) of imidazole is dissociative along the N–H stretch coordinate and may become populated through vibronic coupling with the $\pi\pi^*$ states, or indirectly *via* internal conversion from the $2^1A'(\pi\pi^*)$ state (see Fig. 1 for an example of the low lying electronic states). The early electronic structure work for imidazole provided excitation energies between electronic states and helped to characterise the lowest energy excited states, the orbitals involved, and oscillator strengths to aid identification in experimental spectra.[11,12] Subsequent analysis of conical intersections by Barbatti *et al.* revealed puckering of the ring upon deactivation from the $\pi\pi^*$ states.[13] This effect was further emphasised a couple of years later with surface hopping calculations by

[a] *School of Chemistry, University of Leeds, Leeds LS2 9JT, UK. E-mail: C.C.Symonds@leeds.ac.uk, D.Shalashilin@leeds.ac.uk*
[b] *School of Earth and Environment, University of Leeds, Leeds LS2 9JT, UK*
[c] *School of Mathematics, University of Bristol, Bristol BS8 1TW, UK*
[d] *Department of Chemistry, University of Warwick, Coventry CV4 7AL, UK*

† Electronic supplementary information (ESI) available. See DOI: 10.1039/c9cp00039a

‡ Present address: Combustion Research Facility, Sandia National Laboratories, Mail Stop 9055, Livermore, CA, 94551-0969, USA.
§ Present address: Consiglio Nazionale delle Ricerche, Istituto di Biostrutture e Bioimmagini (CNR-IBB), *via* Mezzocannone 16, 80136, Napoli, Italy.

Published on 17 April 2019. Downloaded by CONSIGLIO NAZIONALE DELLE on 3/14/2022 6:54:14 PM.

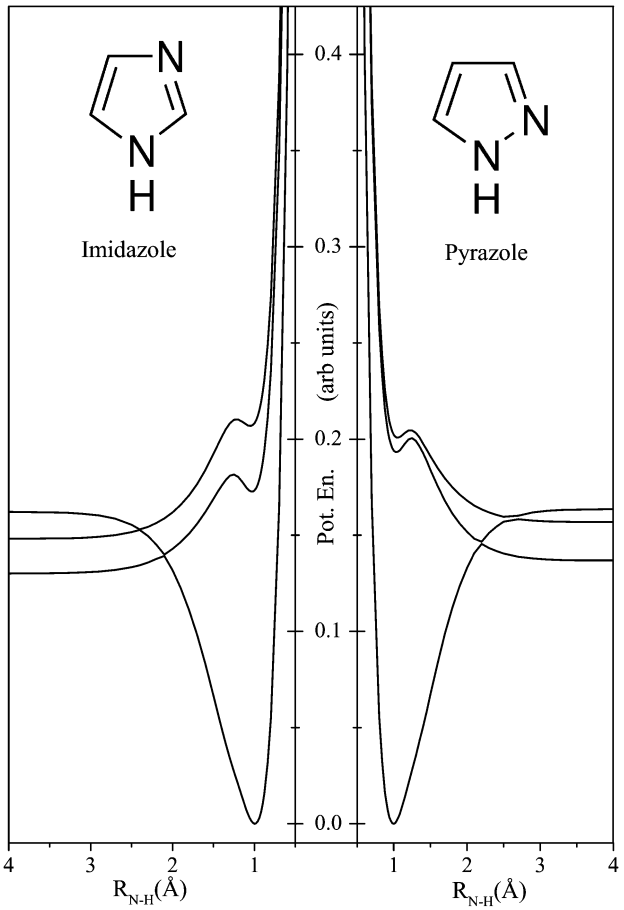

Fig. 1 Schematic of the potential energy curves for imidazole and pyrazole along the R_{N-H} coordinate. The potential energy curves are calculated with CASSCF on the same level as detailed in Section 2 for the three lowest energy states and then offset to place the bottom of the ground states for both molecules at zero. Due to state mixing the S_1 state is of $\pi\pi^*$ character in the Franck–Condon region and as such the low lying $\pi\pi^*$ state for pyrazole is not explicitly shown.

Crespo-Otero *et al.*, where 16% of trajectories were found to be deactivated by this mechanism when initiated in an energy window of 6.0–6.2 eV, placing them mostly on $\pi\pi^*$ states with the rest relaxing through N–H dissociation.[8]

A H Rydberg atom photofragment translational spectroscopy (HRA-PTS) study in the wavelength range $193.3 \leq \lambda \leq 240$ nm by Devine *et al.*[7] on imidazole revealed that excitation to the $1^1A''(\pi\sigma^*)$ state is dominant in the longer wavelength region, whilst at $\lambda < 220$ nm excitation to the $2^1A'(\pi\pi^*)$ state is dominant. In the TKER spectrum a high kinetic energy peak from rapid dissociation of the hydrogen atom was observed and ascribed to the repulsive $1^1A''(\pi\sigma^*)$ state, alongside a lower and broader kinetic energy peak, believed to be due to dissociation following internal conversion to the ground state, which becomes more prevalent at shorter wavelengths. A two-colour time-resolved photoelectron spectroscopy (TR-PES) study by Crespo-Otero *et al.* on imidazole found time-constants to reach the $1^1A''(\pi\sigma^*)$/ground state conical intersection after initial ionisation to the D_0 cation at the beginning of dynamics by pump pulses of $\lambda = 239.6$ nm and $\lambda = 200.8$ nm.[8] These were found to be 17 ± 15 fs and 50 ± 15 fs for the longer and shorter wavelength pulses respectively. The longer time constant from the shorter wavelength pulse was suggested to be due to the internal conversion from $2^1A'(\pi\pi^*)$ to $1^1A''(\pi\sigma^*)$ before reaching the $1^1A''(\pi\sigma^*)$/ground state conical intersection. Additional time-resolved studies at a pump pulse of $\lambda = 200$ nm were carried out by Hadden *et al.*[9] using time-resolved velocity map imaging (TR-VMI) and by Yu *et al.*[10] by measurements of the time-resolved ion yield (TR-IY). They found time constants for the high and low kinetic energy H's of 78 ± 37 and 163 ± 50 fs; and 82 ± 30 and 199 ± 30 fs, respectively. This relatively fast timescale for the low kinetic energy H's led to the suggestion that the appearance of the low KE H atoms was due to multiphoton pump processes. A longer dissociation time of $\tau_{obs} > 270$ ps was found through TR-VMI measurements by Roberts *et al.*[3] which was assigned to dissociation of H atoms following internal conversion to the ground state. The H atoms detected in that work were determined to be from N–H bond rupture rather than from the C–H bond, due to a negligible amount of H atoms produced with imidazole-d_1.

Pyrazole differs from imidazole in that the position of the nitrogen atom in the aromatic ring is shifted from the 3 position to the 2 position, creating an N–N bond. Pyrazole also differs from imidazole in that the lowest energy $\pi\pi^*$ state ($2^1A'$) lies below the lowest energy $\pi\sigma^*$ state ($1^1A''$), meaning at long wavelengths it is the $\pi\pi^*$ state that is populated initially.[19,20] In comparison to investigations of imidazole, experimental studies of pyrazole are relatively sparse. A similar HRA-PTS study to that carried out by Devine *et al.* on imidazole was performed by King *et al.* on pyrazole in the $193.3 \leq \lambda \leq 230$ nm range, finding that excitation to the $2^1A'(\pi\pi^*)$ state is dominant in the longer wavelength region, whilst excitation to $1^1A''(\pi\sigma^*)$ predominantly occurred at $\lambda < 214$ nm.[15] The slow, lower energy distribution in the H atom TKER spectrum was therefore shown to be dominant at longer wavelengths, whilst the faster, higher energy distribution increased in intensity at shorter wavelengths. The loss of a H atom means the pyrazolyl radicals are of C_{2v} symmetry rather than the C_s symmetry of the pyrazole molecule. This change in symmetry is also true for imidazole; however while the ground state of the imidazolyl radical is of 1^2B_1 symmetry,[6] the pyrazolyl radical has ground states of 1^2A_2 symmetry. However, the gap between the 1^2A_2 and 1^2B_1 levels is small in pyrazolyl, meaning the photoproducts are formed in a mixture of states.[15] Investigations of pyrazole were carried out by Williams *et al.*,[16] who used TR-VMI to investigate N–H dissociation and find H atom appearance lifetimes for pyrazole following $\lambda = 200$ nm excitation, finding that the high kinetic energy H atoms had an appearance lifetime of <50 fs, and the low kinetic energy H atoms due to multiphoton processes had an appearance lifetime of 112 ± 34 fs. In the same article, they also considered relaxation through ring deformation and photofragmentation using TR-IY measurements analysed using a model based on calculations of imidazole, finding that only 4–13% of trajectories relax through ring-puckering or ring-opening and concluding that ring deformation was only a

 This journal is © the Owner Societies 2019

Published on 17 April 2019. Downloaded by CONSIGLIO NAZIONALE DELLE on 3/14/2022 6:54:14 PM.

minor relaxation pathway in pyrazole, with N–H bond rupture along the $^1\pi\sigma^*$ state being the major pathway. Later work by Roberts *et al.* reported a lifetime for dissociation of the N–H bond following internal conversion to the ground state of τ_{obs} 193 ± 35 ps for pyrazole, and also determined the source of the high kinetic energy H atoms from dissociation to originate from the N–H bond rather than from the C–H bond through TR-VMI measurements of pyrazole-d_1 and pyrazole-d_3.[3]

Theoretical investigations of pyrazole are similarly sparse, particularly the consideration of dynamics. Calculations using the complete active space second order perturbation theory (CASPT2) have been used to characterise the low lying electronic states of pyrazole,[15] and Xie *et al.*[17] have used surface hopping combined with MS-CASPT2(10,8) electronic structure calculations to investigate dynamics of the S_1 state. While the MS-CASPT2 calculations found the S_1 state to be of $\pi\pi^*$ character in the Franck–Condon region in agreement with experiment, and found barrierless conversions to repulsive $\pi\sigma^*$ character along both N–H and N–N stretch coordinates, with a subsequent conical intersection with S_0, surprisingly the surface hopping dynamics calculations only saw the N–N bond stretch as a relaxation pathway in disagreement with the conclusions made by Williams *et al.* and King *et al.* in their previous experimental work. A second relaxation pathway to the S_0 state was found through the ring puckering coordinate, with a branching ratio of 93 : 7 in favour of ring opening *via* the N–N bond, and the calculations determined the $^1\pi\sigma^*$ relaxation along the N–H bond to be almost entirely suppressed. To explain the N–H dissociation seen in experimental results, Xie *et al.* suggested that the detected H atom signal was a result of dissociation after relaxation to the S_0 state, even those components of the signal with very rapid dissociation lifetimes.

While experimental studies have been conducted to compare the structural isomers imidazole and pyrazole directly on an even footing,[3,4] such a comparison has not been carried out theoretically, nor has a theoretical comparison of the effect of selective deuteration of the N–H bond for the two molecules. To carry out these calculations we use the *ab initio* multiple cloning (AIMC)[21] method which has previously been used to study the similar molecules pyrrole[22,23] and 2-ethylpyrrole.[24] AIMC is an *ab initio* direct dynamics version of the Multiconfigurational Ehrenfest (MCE) approach[25] which uses frozen Gaussian basis functions (or equivalently, coherent states) guided by Ehrenfest trajectories to describe the nuclear wavepacket. The electronic potential energy surfaces are calculated at the centres of these Gaussian basis functions as the simulation is running, or ''on the fly'', to provide a fully dimensional and accurate description of nonadiabatic dynamics. The method also incorporates basis function cloning, a description of wavepacket splitting similar to that of *ab initio* multiple spawning (AIMS),[26–29] and in our previous work[25,30] it has been demonstrated that for model systems comprised of tens of degrees of freedom the inclusion of this cloning process allows MCE simulations to converge to results which agree with numerically exact benchmarks.

2 Computational details

Simulations were carried out using the AIMC method, an *ab initio* quantum direct dynamics method based on the successful Multiconfigurational Ehrenfest (MCE) method which includes basis function cloning. An accounting of the working equations of the AIMC method and a description of the cloning procedure included in the method are given in the ESI.† As with previous AIMC studies,[21–23] dynamics were simulated using a modified version of the AIMS-MOLPRO package[29,31,32] that incorporates Ehrenfest trajectories to guide the quantum basis set. The electronic structure calculations were performed using CASSCF with Dunning's cc-PVDZ set,[33] with the additions of one diffuse *s* function, one set of *p* functions and one set of *d* functions on the nitrogen atom attached to the dissociative hydrogen/deuterium, and additions of one diffuse *s* function and a set of *p* functions to the dissociative hydrogen/deuterium atom for both molecules in this study. The use of these extra diffuse functions rather than using the full aug-cc-pVDZ basis set ensured that the dynamics under investigation were properly described while also limiting the computational expense of the simulations themselves which ran to over 2.5×10^5 hours of processor time for the full set of trajectories across all molecules investigated. A discussion of the validity of this reduction in the basis set is given in the ESI.† The active spaces used for both molecules consisted of 10 electrons in 8 orbitals (three ring π orbitals and two corresponding π^* orbitals, the N–H/D σ and corresponding σ^* orbital, and the lone pair on the nitrogen atom). State averaging and dynamics were performed over three states – the ground and two lowest excited singlet states. The width of the Gaussian basis functions, γ, was taken to be 4.7 Bohr^{-2} for hydrogen, 6.6 Bohr^{-2} for deuterium, 22.7 Bohr^{-2} for carbon and 19.0 Bohr^{-2} for nitrogen as suggested in ref. 34.

Initial positions and momenta for the nuclei were sampled from the ground state vibrational Wigner distribution in the harmonic approximation using vibrational frequencies and normal modes calculated at the same level of CASSCF theory for each molecule as above. Excitation from the ground to the first excited state is approximated by placing the trajectory-guided basis functions on the excited electronic state surface. It is understood that the finer details of initial photoexcitation are not completely accounted for by this approximation, and work has recently been presented by this group which endeavours to simulate the initial excitation pulse more accurately for future calculations.[35]

A total of 1000 trajectories were used for both molecules and the same numbers for their deuterated species with dynamics starting on the first excited state for all simulations. These trajectories are used to guide the basis sets of coupled Ehrenfest configurations in the wavefunction, as described further in the ESI.† Simulated data were compared to experimental results obtained using a 200 nm pump pulse to excite the molecules. This pulse served to excite imidazole to the first excited state directly and to excite pyrazole to the second excited state; however after excitation pyrazole undergoes rapid decay to the first excited state as described by King *et al.*[15] and

Published on 17 April 2019. Downloaded by CONSIGLIO NAZIONALE DELLE on 3/14/2022 6:54:14 PM.

Table 1 Table of the total basis function cloning and dissociation for all molecules

Molecule	Number of cloned basis functions	Percentage of dissociative basis functions
Imidazole	209	79%
Imidazole-d_1	48	84%
Pyrazole	80	88%
Pyrazole-d_1	18	86%

also as discussed in the ESI.† Calculations were run for 200 fs for all molecules using a timestep of ~0.6 fs (2.5 a.u.), or until the N–H/D bond exceeded 4 Å, which was defined as the point of dissociation. The amount of basis function cloning experienced for each molecule, along with the fraction of basis functions that were dissociative within 200 fs, is given in Table 1. The rate of cloning is greatly influenced by the layout of the potential energy surfaces, and this can be seen in the differences between the cloning rates for imidazole and pyrazole. For both deuterated species, a lower rate of cloning is seen compared to their undeuterated molecules which is thought to be due to the lower vibrational frequency from the N–D bond resulting in fewer conical intersections being encountered along the N–H/D coordinate.

3 Results

The analysis of the dissociation dynamics of imidazole, pyrazole and their selectively deuterated derivatives is carried out using a method originally developed and applied in ref. 24. For each of the molecules studied, the H and D atom TKER spectra are presented and compared to experimental data as well as to each other. The kinetic energies of dissociated H/D atoms obtained from the calculation are smoothed with Gaussian functions (σ = 200 cm^{-1}) to create a curve for the TKER spectrum, as opposed to a stick spectrum of delta functions, which allows better comparison to time resolved experimental results. This procedure has been used in previous publications to obtain simulated TKER spectra from AIMC calculations.[22–24] In addition to the TKER spectra, normalised sums over dissociated basis functions are presented and, after a smoothing procedure that takes into account the pump and probe temporal widths, these are used to calculate the dissociation time constants. The smoothing procedure has been discussed previously in ref. 24 and 36 and is necessary for any direct comparison to experimental results as the simulation has well defined start and end points while the temporal widths of the laser pulses ''blur'' these points in the experimental results. For the smoothing process the pump and probe laser pulses are assumed to be Gaussian in time, with temporal widths of σ_{pump} and σ_{probe} respectively, parameters that were determined for the experimental data by taking the time resolved non-resonant ionisation of NH_3 to be the cross correlation of the two laser pulses (usually ~50–100 fs), as explained in ref. 16. The raw dissociation times are then converted to Gaussian probability distributions with widths equal to the convolution of the pump and probe pulses. The probe consists of 2 + 1 resonance enhanced multi-photon ionisation (REMPI) of H atom photofragments, and so for the probe pulse this simultaneous absorption of 3 photons will reduce the Gaussian probability distribution that models it by a factor of $\sqrt{3}$. A cumulative sum of these Gaussian distributions is then computed for all trajectory-guided basis functions, weighted to account for the contributions due to cloned basis functions. This allows a smoothed transient to be generated which can be compared directly to renormalised experimental data that have had a time zero correction applied such as carried out in ref. 37. This smoothed transient is then fitted to the kinetic model employed by Stavros *et al.* in the same reference and elsewhere, and by fitting this model to the experimental data also, the H/D appearance lifetimes can be calculated and compared for both the simulated and experimental data. The kinetic model is given by an exponential rise with time constant τ multiplied by the Heaviside unit step function $u(t - t_0)$, convoluted with a Gaussian instrument response function $G_{\mathrm{IRF}}(t - t_0)$ and multiplied by an amplitude A, with a term S_0 to account for any vertical offset.

$$S(t - t_0) = S_0 + A[G_{\mathrm{IRF}}(t - t_0) \times ((1 - \mathrm{e}^{-(t-t_0)/\tau})u(t - t_0))]. \quad (1)$$

3.1 Imidazole

TKER spectra for imidazole and imidazole-d_1 are given in Fig. 2 with the experimental TKER spectra for these two molecules given in the inset. The experimental spectrum for imidazole was published previously by Roberts *et al.*[3] and the imidazole-d_1 spectrum is from unpublished data from the same group.[38] The experimental data were obtained through REMPI probing of H/D atoms generated following excitation by a 200 nm pump pulse at Δt = 2.5 ps for imidazole and at Δt = 600 ps for imidazole-d_1. Due to differences in zero point energy between

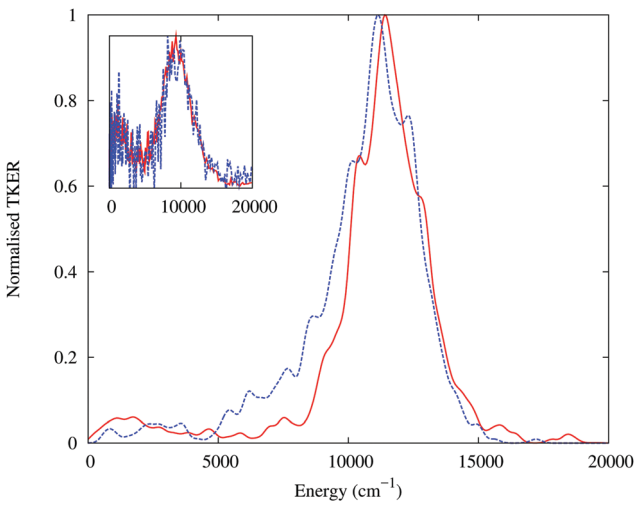

Fig. 2 Calculated H atom TKER spectrum for imidazole (solid red) compared against the D atom TKER spectrum for imidazole-d_1 (dashed blue); experimental results at a pump wavelength of λ = 200 nm are shown in the inset.

This journal is © the Owner Societies 2019

Published on 17 April 2019. Downloaded by CONSIGLIO NAZIONALE DELLE on 3/14/2022 6:54:14 PM.

imidazole and its selectively deuterated species, a shift in the peak of the spectrum towards lower energy would be expected. While such a shift is visible in the AIMC results, it is much smaller than the $\sim$900 cm^{-1} shift that was seen recently in AIMC simulations of 2-ethylpyrrole.[24] It is also difficult to see a shift in the experimental TKER spectrum for imidazole-d_1. This is most likely due to "above origin" excitation in the experimental data, where the higher vibrational modes are populated by the pump pulse during excitation of the molecules. This has the effect of suppressing the shift in the high energy peak of the TKER spectrum for deuterated molecules. While a low energy peak is seen in the experimental result only a small intensity is seen in the low energy region for the calculated spectra. This peak is explained by Roberts *et al.*[3] as due to multiphoton processes, which the AIMC simulations do not consider, and as such the lack of a low energy peak is exactly as one would expect. Furthermore, for long pump–probe delays the low KE structure becomes more pronounced, whereas in the calculations 79% of imidazole basis functions and 84% of imidazole-d_1 basis functions are dissociated by 200 fs, meaning that this significant increase in intensity is unlikely to occur. The high energy peak is shifted up in energy with respect to the experimental data by approximately 2000–2500 cm^{-1}. This behaviour is understood to be due to inaccuracies in the CASSCF potential energy surfaces as they overestimate the gap between excited states in the Franck–Condon region and the ground state in the asymptotic N–H dissociative stretch region. This shift is therefore expected with similar shifts seen in earlier results for the simulated photodissociation of pyrrole[22,23] and 2-ethylpyrrole.[24]

Fig. 3 gives the H-atom appearance lifetime for imidazole (A) and the D-atom appearance lifetime for imidazole-d_1 (B) based on the AIMC calculations alongside appearance lifetimes from experimental results.[38] To obtain the appearance lifetimes a smoothing process is carried out on the raw AIMC data as detailed above using pump and probe pulse widths of σ_{pump} = 62 fs and $\sigma_{\mathrm{probe}} = 37/\sqrt{3}$ fs for both imidazole and imidazole-d_1 which are chosen to agree with the experimental cross correlation between pump and probe of σ_{xc} = 72 fs. The kinetic model is fitted to both the smoothed data and to the experimental data to obtain the appearance lifetimes (although a modification is made for the imidazole-d_1 data as detailed below). Examples of the transients with the kinetic fit applied are given in the ESI.† The two appearance lifetimes for imidazole show an excellent agreement with each other, with a calculated H-atom lifetime of τ_{NH} = 49.4 $\pm$ 0.3 fs and an experimental lifetime of τ_{NH} = 51 $\pm$ 2 fs based on renormalised data. These lifetimes are both within the error margin of the previously reported value of Hadden[9] of τ_{NH} = 78 $\pm$ 37 fs and very close to the error margin of the value measured by Yu[10] of τ_{NH} = 82 $\pm$ 30 fs for high kinetic energy H atoms. The values are also particularly close to the lower of the values measured by Crespo-Otero *et al.*[8] of τ_{NH} = 50 $\pm$ 15 fs for excitation by λ = 200.8 nm to the D_0 cation. For imidazole-d_1 the agreement between the experimental and calculated lifetimes is not quite as close but still good, with a D-atom appearance lifetime of τ_{ND} = 70.9 $\pm$ 0.6 fs from AIMC calculations

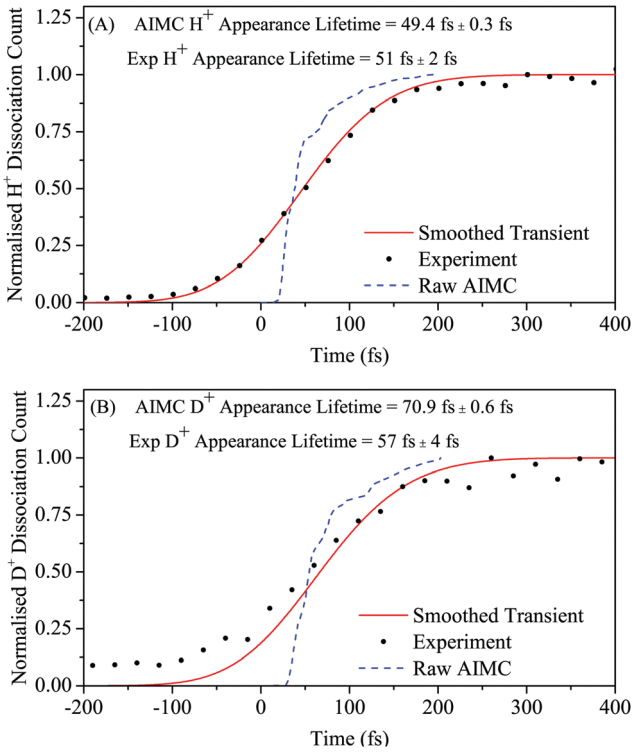

Fig. 3 Raw cumulative sum of dissociation times from trajectory-guided basis functions, alongside smoothed H and D atom appearance transients and experimental data for (A) imidazole and (B) imidazole-d_1.

compared to a lifetime of τ_{ND} = 57 $\pm$ 4 fs from experimental results. In the experimental data for imidazole-d_1 there appears to be a vertical offset in the region before t = 0. This has been explained elsewhere[24,37,39,40] as being due to "reverse dynamics" in which the probe pulse acts as a pump to photoexcite the molecule, and then supplies two photons in the 2 + 1′ REMPI scheme for the dissociated H atom, while the third photon is provided by the "pump" pulse. The offset is accounted for in the calculation of the experimental D-atom appearance lifetime by including a reverse time term in the equation for the kinetic model such that

$$S(t) = S_0 + A\left[G_{\mathrm{IRF}}(t-t_0) \times \left(\left(1-\mathrm{e}^{-(t-t_0)/\tau}\right)u(t-t_0)\right)\right] + B\left[G_{\mathrm{IRF}}(t_0-t) \times \left(\left(1-\mathrm{e}^{-(t_0-t)/\tau_{\mathrm{rev}}}\right)u(t_0-t)\right)\right]. \quad (2)$$

Using this model with an allowance for the reverse dynamics seen in the experimental data allows the rise time τ to be extracted unaffected by the offset, which is then compared directly to the value from the AIMC calculations, thus overcoming any disagreement that would be caused by the effects of this offset. Despite this there is still a noticeable disagreement between the appearance lifetimes from the experimental and AIMC data, which is most likely due to inaccuracies in the measured value for t_0 with the imidazole-d_1 data. The appearance lifetimes give a kinetic isotope effect of KIE = 1.43 $\pm$ 0.01

Published on 17 April 2019. Downloaded by CONSIGLIO NAZIONALE DELLE on 3/14/2022 6:54:14 PM.

from AIMC calculations compared to a kinetic isotope effect of KIE = 1.1 ± 0.1 from the experimental measurements. This disagreement in the KIE is again most likely due to the t_0 value for the imidazole-d_1 data. The relatively small KIE is due to there being a very small barrier to dissociation along the S_1 state which the trajectory-guided basis functions are able to get around without the need for tunnelling as shown in Fig. 1, meaning that only the classical $\sqrt{2}$ kinetic isotope effect would be seen.

It should be noted that when considering the appearance lifetimes, one must remember that they can be affected not only by the choice of zero time correction in the case of the experimental data as posited above, but also by the choice of the length of the N–H/D bond at which it is deemed to be dissociated for the AIMC results. In the experimental data, the value of t_0 is chosen based on the same non-resonant ionisation of NH_3 as used to find the temporal pulse widths and a shift in this value would introduce a similar shift in the experimental transient.¶ For the AIMC data, the point of dissociation is taken as being when $R_{N-H/D}$ = 4.0 Å; however increasing or decreasing this distance would similarly increase or decrease the time taken to reach dissociation. One encouraging factor that would indicate that the transients are temporally positioned properly is the agreement in the slopes of the experimental and simulated transients for imidazole. The experimental and AIMC transients for imidazole-d_1 show a good visual agreement also, although this is modified somewhat by the inclusion of the background signal.

When considering the raw cumulative sum of dissociation times (dotted line), some interesting features can be seen in the sub-50 fs regime that is masked by the temporal widths of the laser pulses in the experimental data. Firstly, no dissociation is seen before ~20 fs for either molecule, with dissociation for imidazole starting at Δt = 15.8 fs and dissociation for imidazole-d_1 starting slightly later at Δt = 26.5 fs due to the lower vibrational frequency of the N–D bond compared to that of the N–H bond. This is simply due to the chosen definition of dissociation as being when $R_{N-H/D} \geq 4.0$ Å and will occur experimentally, although such behaviour cannot be seen directly due to the lack of temporal resolution. More interestingly, between ~20 fs and ~50 fs there is a period of rapid dissociation, where some basis functions prepared with sufficient geometry and energy to dissociate immediately do so, followed by a period of slower dissociation where the remaining basis functions encounter the small local minimum in the Franck–Condon region of the S_1 state shown in the potential energy curves for imidazole (Fig. 1A), and so must continue to sample the PES to find a way around the barrier before relaxing to the ground state. This two stage process, which is seen more noticeably in the imidazole data than in the case of its deuterated species, cannot be seen directly in the experimental data as the laser pulses give a "blurring" effect; however when the smoothing process is applied to the raw dissociation data from the AIMC calculations the calculated and experimental data are brought into agreement with each other indicating that this effect may be occurring in the experimental data also. The two stage dissociation has been seen also in AIMC simulations of 2-ethylpyrrole, where it is very pronounced.[24]

3.2 Pyrazole

Fig. 4 shows the calculated TKER spectra for pyrazole and pyrazole-d_1, smoothed using the method described earlier. The experimental TKER spectra for these two molecules, both spectra taken using a pump–probe delay of 2.5 ps, originate from the work of Stavros *et al.* with the pyrazole spectrum previously published in ref. 16 and the pyrazole-d_1 spectrum from previously unpublished data from the same group.[38] As with imidazole, the calculated spectra are shifted to higher energies by around 2000–2500 cm^{-1} compared to experimental spectra as a result of inaccuracies in the CASSCF potential energy surfaces. The expected peak shift due to differences in zero point energy as a result of deuteration is very slight in the AIMC generated spectrum, being most noticeable in the left hand tail of the peak. As with imidazole however, this shift cannot be easily seen in the experimental spectra due to "above origin" excitation in the experimental data. The low energy structure in the calculated spectra again does not seem to be as prevalent as seen in the experimental spectra due to the inability of the AIMC simulations to account for multiphoton processes, which are suggested as the source of the low energy H/D atoms by Williams *et al.*[16] This is increasingly likely as, like imidazole and imidazole-d_1, the vast majority of trajectory-guided basis functions undergo dissociation with 88% of pyrazole basis functions dissociating along with 86% of

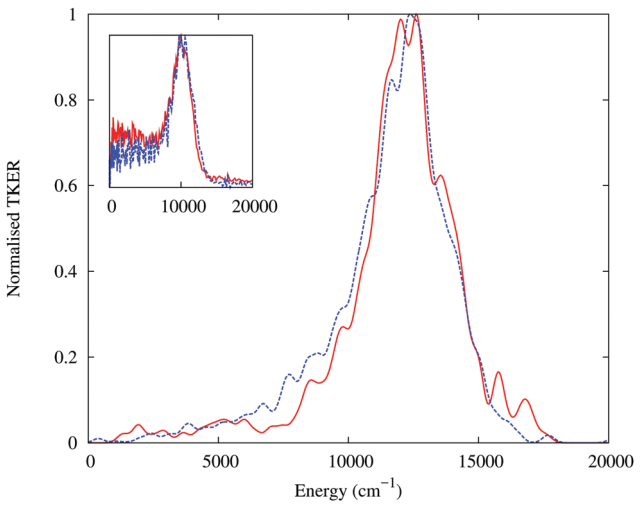

Fig. 4 Calculated H atom TKER spectrum for pyrazole-d_1 (dashed blue) overlaid with that of undeuterated pyrazole (solid red), with experimental results at a pump wavelength of λ = 200 nm in the inset.

¶ There is some uncertainty in the t_0 correction applied to the imidazole and imidazole-d_1 experimental data and so should be treated as an arbitrary shift. This choice of t_0 does not however affect the AIMC data or the slope of the transient rise, only the lateral position of the experimental data and consequently the appearance lifetimes calculated from the experimental data using the kinetic model.

This journal is © the Owner Societies 2019

Published on 17 April 2019. Downloaded by CONSIGLIO NAZIONALE DELLE on 3/14/2022 6:54:14 PM.

pyrazole-d_1 basis functions, and as such a longer simulation is unlikely to result in increased intensity of the low energy peak.

Fig. 5 gives the H-atom appearance lifetime for pyrazole (A) and the D-atom appearance lifetime for pyrazole-d_1 (B) based on the AIMC calculations and compared to those given by fitting to experimental data, with the pyrazole data having been previously published by Williams *et al.*[16] and the pyrazole-d_1 data from unpublished work by the same group.[41] As with imidazole, the raw AIMC data are smoothed using the smoothing process detailed earlier, using σ_{pump} = 62 fs and $\sigma_{probe} = 37/\sqrt{3}$ fs for pyrazole and σ_{pump} = 74 fs and $\sigma_{probe} = 37/\sqrt{3}$ fs for pyrazole-d_1 to match the experimental pump/probe cross correlations of σ_{xc} = 72 fs and σ_{xc} = 83 fs. The smoothed data and the experimental data are both fitted to the kinetic model given by eqn (1) as no background signal from reverse dynamics is seen in either of the experimental data sets. In addition to the lack of a background signal, for the experimental data there is a higher level of certainty regarding the value of t_0 compared to the data for imidazole and its selectively deuterated species. The agreement between the smoothed AIMC transients and the experimental data is visually very good and the agreement between the calculated and experimental lifetimes for pyrazole is similarly good, with a value of 47.6 ± 0.3 fs from the AIMC calculations comparing well to the 42 ± 6 fs lifetime obtained from fitting to the experimental data. It should be noted however that the experimental H^+ appearance lifetime is below the temporal resolution of ~50 fs for the experiment and so can only be reported as τ_{NH} < 50 fs as was done originally.[16] For pyrazole-d_1, a good level of agreement is achieved as for pyrazole, although despite the experimental and AIMC transients visually agreeing very well there is some difference in the D^+ appearance lifetimes with a calculated D-atom appearance lifetime of 63.9 ± 0.7 fs from AIMC calculations compared to a lifetime of 56 ± 3 fs from experimental results. These appearance lifetimes give a fairly small kinetic isotope effect of KIE = 1.34 ± 0.01 from AIMC calculations compared to a kinetic isotope effect of KIE = 1.3 ± 0.2 from the experimental measurements, and due to the higher level of certainty regarding the t_0 corrections for the experimental data this agreement is very encouraging. The values for the KIE are again in the region of $\sqrt{2}$ which would seem to be in agreement with King *et al.*,[15] who suggest a rapid conversion between the low lying ππ* state and the repulsive πσ* state, indicating that no tunneling would occur in the dissociation of pyrazole. The two-step dissociation seen in the raw AIMC dissociation times is similar to that seen for imidazole and imidazole-d_1, although for undeuterated pyrazole the initial rise accounts for a higher proportion of dissociating basis functions than for imidazole or pyrazole-d_1. This behaviour is consistent with the experimental findings in ref. 3 and 16 that direct excitation to the πσ* manifold and the low lying ππ* will result in rapid N–H bond rupture.

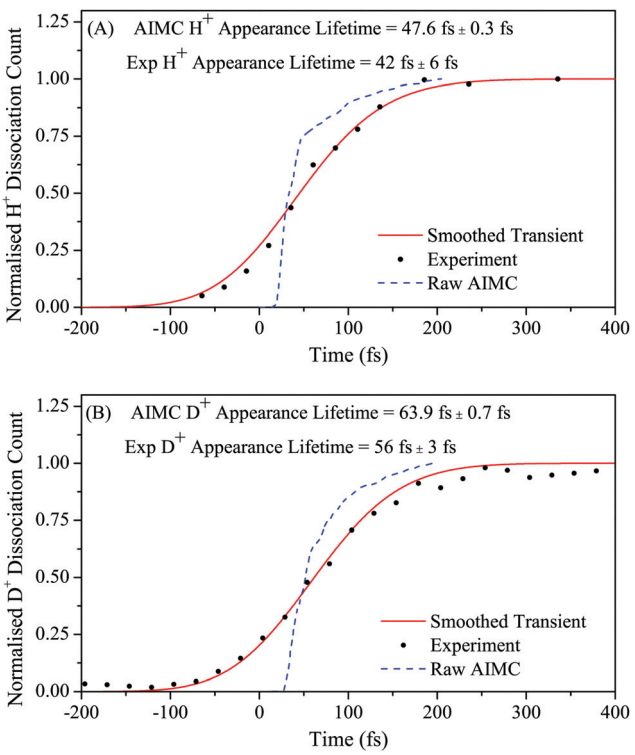

Fig. 5 Raw cumulative sum of dissociation times from trajectory-guided basis functions, alongside smoothed H/D atom appearance transients with associated fits and experimental data for (A) pyrazole and (B) pyrazole-d_1.

At first glance both our results and the experimental results presented in ref. 3 and 16 would seem to be in disagreement with the theoretical work by Xie *et al.*[17] as our results suggest that due to the prevalence of rapid dissociation, as seen by the steep rise in the AIMC raw dissociation data in the region 20 fs $\lesssim t \lesssim$ 50 fs, the dissociation of the N–H/D bond is not suppressed and may in fact be a competitive relaxation pathway. This agreement between our simulations and the experimental results does not mean however that the rupture of the N–N bond can be discounted as a relaxation mechanism, or what the particular branching ratio of the different relaxation mechanisms could be. Indeed when one considers the active spaces used by our simulation and by Xie *et al.*, it can be seen that a simple comparison between these two simulations is not possible. For the simulations carried out in ref. 17 the active space for the MS-CASPT2(10,8) calculations made no inclusion of σ or σ* orbitals on the N–H bond, while a pair of σ and σ* orbitals were included on the N–N bond. As a result, there would be no way to consider, using this active space, whether the N–H bond is significant or not as the calculations would only consider the N–N bond when looking at any dissociation of the bonds in pyrazole. In contrast to this, and similar to the CASSCF/CASPT2(10,9) electronic structure calculations presented by King *et al.*,[15] the active space used for our AIMC simulations contains a pair of σ and σ* orbitals only on the N–H bond but no such pair of σ and σ* orbitals on the N–N bond, which would preclude relaxation through ring-opening *via* the rupture of the N–N bond. As such while the simulations can state that both relaxation mechanisms considered are allowed by the electronic structure of pyrazole, no comment can be made based on either simulation regarding which of the

Published on 17 April 2019. Downloaded by CONSIGLIO NAZIONALE DELLE on 3/14/2022 6:54:14 PM.

proposed bond rupture related relaxation mechanisms is more dominant. A comparison of how different active spaces and basis sets can affect the potential energy curves along the N–H stretch is included in the ESI.† While our simulations are consistent with previous experimental dynamics reported by Williams *et al.*[16] and by King *et al.*,[15] the role of N–N bond rupture could possibly be more important under experimental conditions other than those presented in those articles; indeed recent experimental results in the group of Richard Thomas using TR-PES have given an indication that N–N bond rupture may also play a role in the relaxation mechanics of pyrazole.[42] Therefore, to obtain a suitable branching ratio for both mechanisms, further theoretical studies with electronic structure at a higher level of theory using a larger active space which accounts for both N–H and N–N dissociation would be required.

4 Conclusions

We have used AIMC to simulate fully quantum dynamics for imidazole and pyrazole along with their selectively deuterated species. TKER spectra and H/D atom appearance lifetimes from N–H/D bond rupture have been produced and compared to experimental results.[3,9,10,16,38,41] Qualitatively the TKER spectra agree with experimental data, reproducing the high energy peaks associated with direct dissociation *via* the repulsive $\pi\sigma^*$ state. In the TKER spectra from the AIMC calculations, small kinetic energy shifts in the high kinetic energy peaks of the deuterated molecules are seen due to differences in zero point energy. These shifts are hard to see in the experimental spectra due to "above origin" excitation, where the pump imparts a small amount of excess energy to each molecule, raising the molecule to higher vibrational modes. This reduces the effect of the zero point energy induced shift in the high KE peak of the TKER spectra for the deuterated molecules. The AIMC simulations however excite the molecules entirely to the electronic states with no vibrational excitation, giving the largest depiction of the high energy peak shift. It is curious however that this shift is still very small in comparison to the shifts that were seen experimentally by Cole-Filipiak *et al.*[37] and which have recently been faithfully reproduced by Green *et al.*[24] using AIMC for the 2-ethylpyrrole molecule. Further investigations of the comparative photodynamics of azoles and their deuterated derivatives, both experimental and theoretical, may yield an explanation for this surprisingly small isotopic shift.

The H/D appearance lifetimes were obtained by smoothing the raw AIMC dissociation counts to incorporate the "blurring" effect that results from the temporal widths of the laser pulses. This allowed the theoretical results to be compared directly to the experimental results. By fitting to the experimental and smoothed AIMC dissociation data, figures for the H/D appearance lifetimes could also be found which for the most part gave very good agreement between experimental and AIMC results, with both molecules showing a kinetic isotope effect in the region of $\sqrt{2}$ due to the absence of tunneling. Consideration of the raw AIMC dissociation gave insight into the sub-50 fs dynamics confirming earlier insights from the work of Green *et al.*[24] that showed evidence of a two-step model in the ultrafast photodissociation of 2-ethylpyrrole where molecules with the correct geometry experience over-the-barrier dissociation almost immediately after excitation resulting in an early rapid rise in the dissociation count up to $\geq$60% of dissociative basis functions, while those without the correct geometry must further sample the potential energy surface before dissociation, shown as a second slower rise. The fact that this behaviour, previously seen for 2-ethylpyrrole, is also seen for both imidazole and pyrazole along with their selectively deuterated species indicates that an ultrafast, two-step photodissociation mechanism may be common along low lying repulsive $\pi\sigma^*$ states.

Our results confirm the importance of N–H bond rupture and the repulsive $^1\pi\sigma^*$ state along this coordinate in the relaxation of imidazole, and give weight to the conclusions made by both Williams *et al.*[16] and King *et al.*[15] regarding the direct ultrafast dissociation of the N–H bond in pyrazole. This would appear to be at odds with the conclusions drawn by Xie *et al.*,[17] who suggested that the N–H bond dissociation is almost entirely suppressed as a relaxation mechanism in pyrazole and instead it is the rupture of the N–N bond that plays a dominant role in the photodynamics. Contrary to this our results indicate that pyrazole may behave in a similar fashion to other nitrogen containing heteroaromatic molecules such as imidazole where the N–H bond breaks extremely quickly, indicating that, as with imidazole, this bond rupture could provide a competitive relaxation mechanism in pyrazole. The excellent agreement with the experimental results of Williams *et al.*[16,41] and the fast dissociation times for high KE H atoms seen in both the experimental results and the AIMC simulations could be evidence, albeit indirect, that the H atoms are produced by direct dissociation of the N–H bond. As discussed in Section 3.2 however, the fact that the present calculations differ from those of Xie *et al.* cannot be seen as any indication of the dominance of one relaxation mechanism over the other as, due to the differences in the structure of the active space used in the respective calculations, neither simulation can fully describe both mechanisms. As such we are unable to make any conclusions as regards the relative branching ratios, and to make such a comparison further simulations would be needed at a higher level of electronic structure theory with a larger active space.

In this work the AIMC method has been used to give the first fully quantum theoretical treatment of pyrazole and imidazole on an equal footing, and the first ever fully quantum theoretical treatments of these molecules' selectively deuterated species, and through this we have been able to give insight into experimental results, particularly in the sub-50 fs regime that is often inaccessible in ultrafast spectroscopy experiments. The ability of AIMC calculations to reproduce experimental results confirms its status as a powerful tool for the simulation of quantum mechanics in small molecular systems and paves the way towards fully predictive quantum chemistry for larger biomolecules.

Conflicts of interest

The authors have no conflicts of interest to declare.

 This journal is © the Owner Societies 2019

Published on 17 April 2019. Downloaded by CONSIGLIO NAZIONALE DELLE on 3/14/2022 6:54:14 PM.

Acknowledgements

The authors would like to extend their gratitude to Gangalong Cui and Oliver Schalk for very helpful discussions regarding their work. The work in this article has been supported by the Leverhulme trust RPG-2015-190. J. A. G. has been supported by EPSRC grant EP/N007549/1 and previously has been supported by the University Research Scholarship from the University of Leeds, as well as funding from the School of Chemistry, University of Leeds. D. M. is supported by EPSRC grant EP/P021123/1 and also would like to acknowledge the previous support by the EPSRC grant EP/N007549/1. N. C. C. F. thanks the Leverhulme Trust for postdoctoral funding. V. G. S. thanks the EPSRC for equipment grants (EP/J007153 and EP/N010825) and the Royal Society and Leverhulme Trust for a Royal Society Leverhulme Trust Senior Research Fellowship.

References

1 M. N. R. Ashfold, B. Cronin, A. L. Devine, R. N. Dixon and M. G. D. Nix, *Science*, 2006, **312**, 1637–1640.
2 M. N. R. Ashfold, G. A. King, D. Murdock, M. G. D. Nix, T. A. A. Oliver and A. G. Sage, *Phys. Chem. Chem. Phys.*, 2010, **12**, 1218–1238.
3 G. M. Roberts, C. A. Williams, M. J. Paterson, S. Ullrich and V. G. Stavros, *Chem. Sci.*, 2012, **3**, 1192–1199.
4 G. M. Roberts and V. G. Stavros, *Chem. Sci.*, 2014, **5**, 1698–1722.
5 R. Montero, A. P. Conde, V. Ovejas, M. Fernández-Fernández, F. Castaño and A. Longarte, *J. Phys. Chem. A*, 2012, **116**, 10752–10758.
6 A. J. Gianola, T. Ichino, R. L. Hoenigman, S. Kato, V. M. Bierbaum and W. C. Lineberger, *J. Phys. Chem. A*, 2005, **109**, 11504–11514.
7 A. L. Devine, B. Cronin, M. G. D. Nix and M. N. R. Ashfold, *J. Chem. Phys.*, 2006, **125**, 184302.
8 R. Crespo-Otero, M. Barbatti, H. Yu, N. L. Evans and S. Ullrich, *ChemPhysChem*, 2011, **12**, 3365–3375.
9 D. J. Hadden, K. L. Wells, G. M. Roberts, L. T. Bergendahl, M. J. Paterson and V. G. Stavros, *Phys. Chem. Chem. Phys.*, 2011, **13**, 10342–10349.
10 H. Yu, N. L. Evans, V. G. Stavros and S. Ullrich, *Phys. Chem. Chem. Phys.*, 2012, **14**, 6266–6272.
11 F. B. C. Machado and E. R. Davidson, *J. Chem. Phys.*, 1992, **97**, 1881–1891.
12 L. Serrano-Andrés, M. P. Fülscher, B. O. Roos and M. Merchán, *J. Phys. Chem.*, 1996, **100**, 6484–6491.
13 M. Barbatti, H. Lischka, S. Salzmann and C. M. Marian, *J. Chem. Phys.*, 2009, **130**, 034305.
14 J. Pittner, H. Lischka and M. Barbatti, *Chem. Phys.*, 2009, **356**, 147–152.
15 G. A. King, T. A. A. Oliver, M. G. D. Nix and M. N. R. Ashfold, *J. Chem. Phys.*, 2010, **132**, 064305.
16 C. A. Williams, G. M. Roberts, H. Yu, N. L. Evans, S. Ullrich and V. G. Stavros, *J. Phys. Chem. A*, 2012, **116**, 2600–2609.
17 B.-B. Xie, X.-Y. Liu, Q. Fang, W.-H. Fang and G. Cui, *J. Phys. Chem. Lett.*, 2017, **8**, 1019–1024.
18 A. L. Sobolewski, W. Domcke, C. Dedonder-Lardeux and C. Jouvet, *Phys. Chem. Chem. Phys.*, 2002, **4**, 1093–1100.
19 I. Walker, M. Palmer, M.-J. Hubin-Franskin and J. Delwiche, *Chem. Phys. Lett.*, 2003, **367**, 517–522.
20 M. H. Palmer and M. F. Guest, *Chem. Phys.*, 2003, **291**, 287–306.
21 D. V. Makhov, W. J. Glover, T. J. Martínez and D. V. Shalashilin, *J. Chem. Phys.*, 2014, **141**, 054110.
22 D. V. Makhov, K. Saita, T. J. Martínez and D. V. Shalashilin, *Phys. Chem. Chem. Phys.*, 2015, **17**, 3316–3325.
23 D. V. Makhov, T. J. Martínez and D. V. Shalashilin, *Faraday Discuss.*, 2016, **194**, 81–94.
24 J. A. Green, D. V. Makhov, N. C. Cole-Filipiak, C. Symonds, V. G. Stavros and D. V. Shalashilin, *Phys. Chem. Chem. Phys.*, 2019, **21**, 3832–3841.
25 D. V. Makhov, C. Symonds, S. Fernandez-Alberti and D. V. Shalashilin, *Chem. Phys.*, 2017, **493**, 200–218.
26 T. J. Martínez, M. Ben-Nun and R. D. Levine, *J. Phys. Chem.*, 1996, **100**, 7884–7895.
27 M. Ben-Nun, J. Quenneville and T. J. Martínez, *J. Phys. Chem. A*, 2000, **104**, 5161–5175.
28 M. Ben-Nun and T. J. Martínez, *Adv. Chem. Phys.*, 2002, **121**, 439–512.
29 B. G. Levine, J. D. Coe, A. M. Virshup and T. J. Martínez, *Chem. Phys.*, 2008, **347**, 3–16.
30 C. Symonds, J. A. Kattirtzi and D. V. Shalashilin, *J. Chem. Phys.*, 2018, **148**, 184113.
31 H.-J. Werner, P. J. Knowles, G. Knizia, F. R. Manby, M. Schütz, *et al.*, *MOLPRO, version 2010.1, a package of ab initio programs*, 2010, see http://www.molpro.net.
32 H.-J. Werner, P. J. Knowles, G. Knizia, F. R. Manby and M. Schütz, *Wiley Interdiscip. Rev.: Comput. Mol. Sci.*, 2012, **2**, 242–253.
33 T. H. Dunning Jr., *J. Chem. Phys.*, 1989, **90**, 1007–1023.
34 A. L. Thompson, C. Punwong and T. J. Martínez, *Chem. Phys.*, 2010, **370**, 70–77.
35 D. V. Makhov and D. V. Shalashilin, *Chem. Phys.*, 2018, **515**, 46–51.
36 N. d. N. Rodrigues, N. C. Cole-Filipiak, K. N. Blodgett, C. Abeysekera, T. S. Zwier and V. G. Stavros, *Nat. Commun.*, 2018, **9**, 5188.
37 N. C. Cole-Filipiak, M. Staniforth, N. d. N. Rodrigues, Y. Peperstraete and V. G. Stavros, *J. Phys. Chem. A*, 2017, **121**, 969–976.
38 G. M. Roberts, C. A. Williams, M. J. Paterson, S. Ullrich and V. G. Stavros, 2012, unpublished work.
39 H. Lippert, H.-H. Ritze, I. V. Hertel and W. Radloff, *ChemPhysChem*, 2004, **5**, 1423–1427.
40 G. M. Roberts, C. A. Williams, H. Yu, A. S. Chatterley, J. D. Young, S. Ullrich and V. G. Stavros, *Faraday Discuss.*, 2013, **163**, 95–116.
41 C. A. Williams, G. M. Roberts, H. Yu, N. L. Evans, S. Ullrich and V. G. Stavros, 2012, unpublished work.
42 T. Geng, *Excited-state dynamics of small organic molecules studied by time-resolved photoelectron spectroscopy*, PhD thesis, Stockholm University, 2017.